Sociedad Mexicana de Ingeniería Mecánica
Fecha de recepción: xx-xx-2018
Fecha de aceptación: xx-xx-2018

INGENIERÍA MECÁNICA
TECNOLOGÍA Y DESARROLLO
Vol. 6 No. 3 (2018) 107 - 121

Computational Modeling of Direct Steam Generation in Pipes Receiving Concentrated Solar Radiation

Modelación Computacional de la Generación Directa de Vapor en Tuberías que reciben Radiación Solar Concentrada

V.M. Maytorena, J.F. Hinojosa*
Universidad de Sonora (UNISON), Blvd. Rosales y Luis Encinas,
Hermosillo, CP 83000, Sonora, México.
*Corresponding author: fhinojosa@iq.uson.mx

Abstract

The purpose of this work was to simulate the conditions of direct steam generation in a vertical tube receiving concentrated solar radiation. The modified RPI model was used for the conditions of critical heat flux coupled to a Eulerian two fluid model. The mathematical model was solved with CFD software ANSYS FLUENT v15. The results were validated with experimental data reported in the literature and a parametric study was carried out to determinate the effect of the mass flux, the heat flux incident on the wall and the heat transfer area on: the steam quality, the volumetric fraction and the temperatures of liquid and steam. From the results obtained, it was determined the required conditions to obtain a steam quality of 100%.

Resumen

El propósito de este trabajo fue validar una estrategia numérica capaz de simular condiciones de generación directa de vapor en un tubo vertical. Se utilizó el modelo RPI modificado para condiciones de flujo de calor crítico acoplado a un modelo Euleriano de dos fases, según la bibliografía especializada consultada se seleccionaron los modelos que predijeron los mejores resultados como: lo sitios de nucleación activa, frecuencia y diámetros de desprendimiento de salidas de las burbujas además de los coeficientes de transferencia de calor entre las fases. El modelo matemático se resolvió con el software de CFD ANSYS FLUENT v15. Se validaron los resultados con datos experimentales reportados en la literatura. Se analizó el efecto del flux másico, el flujo de calor incidente en la pared del tubo y el área de transferencia de calor sobre: la fracción volumétrica, la calidad del vapor y las temperaturas del líquido y el vapor. A partir de los resultados obtenidos, se determinaron las condiciones que permiten obtener una calidad del vapor de 100 %.

Keywords:
Direct steam generation, Concentrated solar energy, Computational modelling

Palabras clave:
Generación directa de vapor, energía solar concentrada, modelación computacional

Introduction

The current global energy system that supports the living standard of humanity is one of the most important causes of global climate change. It is estimated that greenhouse gas emissions from burning fossil fuels have caused an increase in the global temperature of the earth, causing significant changes in different natural events such as intensity of hurricanes, droughts, floods, etc. On the other hand, concentrating solar thermal systems (CST) are one of the options inside renewable energies to face this problem and consolidate the era of the emission-free energy system. There are several CST technologies (parabolic trough, central tower, linear Fresnel, Dish-Stirling, etc), however, the solar central tower system (SCT) concept has advantages like readily integration in fossil plants for hybrid operation, higher temperatures (up to 1000 °C) and thereby higher efficiency and may operate using thermal storage for more than 20 hours by day [1]. Some SCT power plants directly use high-pressure water with direct steam generation technology (DSG). The thermal receiver of SCT plants with DSG operates with a bank of vertical tubes which receive concentrated solar energy from the heliostats field.

Hirsch et al. [2] realized a study focused on plants with DSG and found that by eliminating heat exchangers and conventional working fluids (synthetic oils or molten salts), the operating costs can be reduced significantly. In addition, the investment costs are also reduced to the elimination of the intermediate equipment that occupies the conventional CST [3]. C. Prieto et al. [4], reported that there are four solar plants in the world that operate with DSG technology in central tower systems, two with saturated steam (PS10 and PS20), installed in Seville Spain and operating commercially since 2007 and 2009, respectively, and two with superheated steam: Ivanpah Solar Project (located in California, United States and in operation since 2013) and Khi Solar One (located in South Africa and in operation since 2016). In the specialized literature, several numerical studies focused on the direct steam generation (DSG) have been found from concentrated solar energy [5-8], but none of these gives information on the phenomenon of phase change that occurs in SCT systems. The studies of DSG based on Computational Fluid Dynamics (CFD) are briefly described next.

Lobon et al. [9-10], worked with solar systems of parabolic trough collectors with DSG. The authors used the CFD software, STAR-CCM+, and implemented a locally homogeneous biphasic flow (LHM) model. Their results were validated using experimental data from the DISS test facility (Spain). However, due to the homogeneous nature of their model, the flow patterns associated with the boiling process could not be determined. R. Dinsenmeyer et al. [11], conducted a study of the DSG in Fresnel-type thermosolar systems, the authors applied the multiphase volume of fluid model (VOF) and the turbulence model k-ε RNG, the models were solved with the CFD software, ANSYS FLUENT 14.5, this work was realized with the finally to predict the evolution of the biphasic flow pattern. Their results were validated with the experiments of Yang et al. [12], however, the authors say that this paper presents a preliminary and relatively qualitative approach in the description of this problem.

Specialized literature was consulted [13-18] and it was found that the RPI model proposed by Kurul and Podowski [19], is the best candidate to solve phase change systems with subcooled boiling. In a modified extension (non-equilibrium and critical heat flux) of the RPI model, it can reproduce conditions of total phase changes (although in this bibliographical review there are not articles with a total phase change).

Above the literature review indicates the absence of a detailed study where the modified RPI model is implemented for to study the DSG technology in solar concentration systems. Considering the above, in this work the modified RPI model is implemented to study the phenomenon of phase change in a receiver tube of a central tower system with DSG technology. A parametric study was carried out to determinate the effect of the mass flux, the heat flux incident on the wall and the heat transfer area on: the steam quality, the volumetric fraction and the temperatures of liquid and steam.

Methodology

Definition of the problem, physical model and operating conditions

The definition of the problem is illustrated in Fig. 1a, a volume of subcooled water flows on a wall whose temperature is too high for the boiling of the fluid to occur on its surface, even when the average temperature of the total volume of the liquid is below its saturation temperature. This problem is characterized as a case of subcooled boiling or boiling on a hot wall. The heat moves directly from the wall to the liquid, so part of that energy will cause an increase in the temperature of the liquid and part generate steam. The temperature of the liquid will also be increased by the heat exchange of the water-steam interface, causing part of the saturated steam to condense. The point where starts the bubbles formation is known as the onset of nucleate boiling (ONB), after that there are conditions corresponding to a highly subcooled zone with a small fraction of vapor. There is a point where the net vapor generation occurs (NVG), after that exists a slightly subcooled zone where the vapor fraction increases. Finally, the system reaches the saturated boiling where the fluid is at the saturation temperature. Additionally, there may be direct energy exchange between the wall and the vapor and from the vapor to the liquid.

In Fig. 1b, the physical model of the problem to be studied is presented (base case). Subcooled water enters through the lower side of the system and moves to the top through a pipe with internal radius (Ri) of 0.0077 m and length (L) of 2 m, the heat flux (qw) is 0.57 MW/m^2. With a mass flux (G) of 900 kg/m^{2}s, at a pressure (P) of 4.5 MPa and an input temperature (Te) of 471.5 K. The numerical results were validated with the experimental results of Bartolomei and Chanturiya [20]. To study the DSG phenomena and evaluate the selected physical-mathematical models, it was carried out a parametric study, varying the following parameters: G, qw and L (see Table 1).

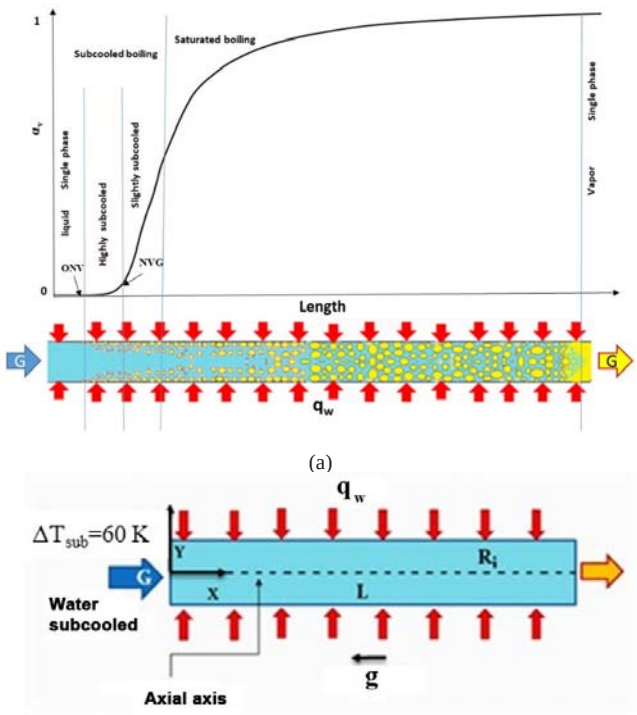

Figure 1 (a) Scheme of the phenomenon of boiling and phase change and (b) Scheme of the physical system.

Table 1. Values of the parametric study.

Cases	G (kg/m^{2}s)	qw (MW/m^2)	L (m)	Re
C1-1 (Base)	900	0.57	2	118,970
C1-2	500	0.57	2	66,094
C1-3	200	0.57	2	26,438
C2-1	900	1.14	2	118,970
C2-2	900	1.71	2	118,970
C3-1	900	0.57	4	118,970
C3-2	900	0.57	8	118,970
C3-3	900	0.57	14	118,970

Mathematical models

Eulerian multiphase model

The mathematical model is based on the equations of continuity, momentum and energy for each phase. The subscript 'k' represents gas or liquid and the subscript 'i' is the non-k phase. The terms α_k, ρ_k, u_k, H_k, represent the volume fraction, density, velocity and specific enthalpy for each phase, respectively. The terms $\dot{m}_{ki}$ and $\dot{m}_{ik}$ represent the mass transfer between phases.

Continuity equation

$$\frac{\partial}{\partial t}\left(\alpha_k \rho_k\right)+\nabla\left(\alpha_k \rho_k \vec{u_k}\right)=\left(\dot{m}_{ki}-\dot{m}_{ik}\right) \tag{1}$$

Momentum equation

$$\begin{aligned}&\frac{\partial}{\partial t}\left(\alpha_k \rho_k \vec{u_k}\right)+\nabla\left(\alpha_k \rho_k \vec{u_k}\vec{u_k}\right)=-\alpha_k \nabla P+\alpha_k \rho_k \vec{g}\\&+\nabla\left(\alpha_k \mu_k^e\left(\nabla\vec{u_k}+\left(\nabla\vec{u_k}\right)^T\right)\right)+\left(\dot{m}_{ki}\vec{u_i}-\dot{m}_{ik}\vec{u_k}\right)\\&+\left(\vec{F_{D,k}}+\vec{F_{L,k}}+\vec{F_{W\,L,k}}+\vec{F_{T\,D,k}}\right)\end{aligned} \tag{2}$$

In equation (2) the first term on the right-hand side represents the pressure force terms. The second term represents the gravity. The third term is a combination of effective viscous stress and turbulent stress term. The fourth term represents gain of momentum due to phase change. Last term represents interfacial forces, and these estimated with the following models: Ishii et al [21], Moraga et al. [22], Antal et al. [23] and Lopez de Bertodano [24], which include drag force, lift force, wall lubrication force, and turbulent dispersion force, respectively.

Energy equation

$$\begin{aligned}&\frac{\partial}{\partial t}\left(\alpha_k \rho_k H_k\right)+\nabla\left(\alpha_k \rho_k \vec{u_k} H_k\right)=\alpha_k \frac{dP_k}{dt}\\&+\nabla\left(\alpha_k\left(\vec{q_k}+\vec{q_k^T}\right)\right)+\left(\dot{m}_{ki}H_i-\dot{m}_{ik}H_k\right)+q_w A_w\end{aligned} \tag{3}$$

In equation (3), the first term on the right-hand side represents the change in enthalpy due to pressure. Second term is a combination of molecular and turbulent heat flux. The third term represents the change in enthalpy due to the diffusive mass flux (evaporation and condensation) and the last term represents the source term that represents the wall heat flux.

Basic RPI wall boiling model

$$q_w = q_c + q_q + q_e \tag{4}$$

The equation (4), is known as the basic RPI model, in this model the total heat flux is divided into three components from the wall to the liquid. The first term on the right side of equation (4) represents the single-phase convective heat flux, qc is used to heat the liquid near the wall and due to heat transfer for convection, the temperature of the liquid near the wall increases to and above the saturation temperature. The heated area of the wall is divided into two parts, one occupied by bubbles in nucleation (A_b) and the rest is covered by liquid (1 - A_b). The mathematical expression for q_c is:

$$q_c = h_c\left(1-A_b\right)\left(T_w-T_l\right) \tag{5}$$

Where h_c represents the single phase convective heat transfer coefficient, T_w is the temperature on the wall y T_l is the average temperature of the bulk liquid. A_b is also called as area of influence and its mathematical expression is as follows:

$$A_b = \min\left(1, K\frac{\pi d_{bw}^2 N_a}{4}\right) \tag{6}$$

The term *K* is obtained with equation (7), was proposed by Del Valle and Kenning [25], d_{bw} is bubble departure diameter and N_a is the nucleation site density.

$$K = 4.8\,e^{\left(\frac{-Ja_{sub}}{80}\right)} \tag{7}$$

Ja_{sub} is the subcooled Jacob number and is defined as:

$$J\,a_{sub} = \frac{\rho_l Cp_l \Delta T_{sub}}{\rho_v h_{lv}} \tag{8}$$

Where ΔT_{sub} is the difference between the saturation temperature (T_{sat}) and the T_l, h_{lv} is the latent heat of vaporization, ρ is the density y Cp is the heat capacity, the subscript indicates the phase, if the subscript is "l" it represents the liquid and if it is "v" it represents the vapor.

The second term of equation (4), represents heat transfer due to quenching. This phenomenon occurs cyclically, first the bubbles are generated, second these begin to grow, third these depart from the wall, and then fresh bulk liquid invade the sites of the liberated bubbles and again new bubbles are formed in those same sites. Mikic and Rohsenow [26] described the mathematical expression for q_q:

$$q_q = A_b\frac{2k_l}{\sqrt{\pi\lambda_l t_w}}\left(T_w-T_l\right) \tag{9}$$

Where k_l is the thermal conductivity, t*w* is waiting period until next bubble appears at same site after bubble departure from nucleation sites on the wall and λ_l is the thermal diffusivity.

The third term of equation (4) represents the heat flux due to evaporation. In this phenomenon the latent heat forms bubbles in the heated wall, which condense on contact with the

subcooled liquid. It is obtained by the following expression:

$$q_e = \dot{V}_v \rho_v h_{lv} = \frac{\pi d_{bw}^3 \rho_v f N_a h_{lv}}{6} \tag{10}$$

Where ($\dot{V}_v$) is the volumetric flow generated on the heated wall and f is bubble departure frequency and it was estimated with Cole's model [27], expressed as follows:

$$f = \frac{\sqrt{4g(\rho_l - \rho_v)}}{3\rho_l d_{bw}} \tag{11}$$

The bubble departure diameter (d_{bw}) is obtain with the Kocamustafaogullari-Ishii's correlation [28]:

$$d_{bw} = 0.0012\left(\frac{\rho_l - \rho_v}{\rho l}\right)^{0.9} 0.0208\varphi\sqrt{\frac{\sigma}{g(\rho_l - \rho_v)}} \tag{12}$$

Where φ is the contact angle of the bubble with heated wall, and σ is the surface tension. Also, is necessary to obtain the diameter of the bubbles (d_b) in the liquid medium.

$$db = \begin{cases} \max\left[1E^{-5}, d_{\min} e^{\left(\frac{-K\Delta T_{sub} - \Delta T_{\max}}{d_{\min}}\right)}\right] \\ \Delta T_{sub} > 13.5K \\ \left[d_{\max} - \mathrm{K}\left(\Delta T_{sub} - \Delta T_{\min}\right)\right] \\ \Delta T_{sub} \le 13.5K \end{cases} \tag{13}$$

Where:

$$K = \frac{d_{max} - d_{min}}{\Delta T_{max} - \Delta T_{min}},\ d_{min} = 0.00015\mathrm{m},\ d_{max} = 0.001\mathrm{m},$$
$$\Delta T_{\max} = 13.15\ \mathrm{K}\ y\ \Delta T_{\min} = 0\ \mathrm{K}$$

The nucleation site density (N_a) is obtained with the Kocamustafaogullari-Ishii's correlation [28]:

$$N_a = \frac{f(\rho^*) R_c^{*-4.4}}{d_{bw}}$$
$$R_c^* = \frac{4\sigma T_{sat}}{d_{bw}\rho_v h_{lv} \Delta T_w} \tag{14}$$
$$\rho^* = \frac{\rho_l - \rho_v}{\rho_v}$$
$$f(\rho^*) = 2.157E^{-7}\rho^{*-3.2}\left(1 + 0.0049\rho^*\right)^{4.13}$$

Modified RPI wall boiling model (RPI modified)

As previously mentioned, the purpose of this study is to analyze theoretically the generation of steam from a subcooled liquid. Therefore, it is necessary to implement a modification to the basic RPI model, because this model (basic RPI), is not focused to simulate conditions where the vapor phase is dominant, because in this model the steam temperature is not calculated from the resolution of the phase energy equation, but instead is fixed at the saturation temperature. To model boiling departing from the nucleate boiling regime (ONB), or to model it up to the critical heat flux and post dry-out condition, it is necessary to include the steam temperature in the solution process. The wall heat partition is now modified, for this case as follows:

$$q_w = \left(q_C + q_q + q_e\right) f(\alpha_l) + \left(1 - f(\alpha_l)\right) q_v \tag{15}$$

Lavieville et al. [29], propose the following mathematical expression:

$$f(\alpha_l) = \begin{cases} 1 - 0.5e^{-20(\alpha_l - \alpha_{l,crit})} \\ \alpha_l \ge \alpha_{l,crit} \\ \left[0.5\left(\frac{\alpha_l}{\alpha_{l,crit}}\right)^{20\alpha_{l,crit}}\right] \\ \alpha_l < \alpha_{l,crit} \end{cases} \tag{16}$$

Here, q_c, q_q, and q_e are the liquid-phase convective heat flux, quenching heat flux, and evaporation heat flux, respectively (described in detail in RPI Model). The extra heat fluxes are q_v representing the convective heat flux of the vapor phase, ($q_v = h_v(T_w - T_l)$), and $\alpha_{l,crit}$=0.2.

In the RPI modified model (critical heat flux, for our case), when $f(\alpha_l)$ approached to 1, the phenomenon is considered as basic RPI wall boiling model. Similarly, the RPI modified model accounts for single phase vapor heat transfer when $f(\alpha_l)$ approached to 0.

Turbulence model

The turbulence of the fluid is model with the standard k-ε model [30]. However, when large or medium bubbles flow through the liquid they leave a wake that generates additional turbulence. The turbulence generated by the bubbles is calculate with the Sato's model [31]. Viscosity due to bubble induced turbulence depends on relative velocity between two phases.

$$\mu_l^{bt} = C_{\mu,bt}\rho_l \alpha_v d_{bo} \left|\overline{u_v} - \overline{u_l}\right| \tag{17}$$

The constant $C_{\mu,bt}$ = 0.6 was obtained experimentally and the term d_{bo} is boiling bubble diameter. The term $|\overline{u_v}\text{-}\overline{u_l}|$, is the relative velocity between two phases.

Interfacial heat transfer

The third term in the energy balance equation (3) represents enthalpy change due to diffusive mass flux i.e. interfacial mass and heat transfer between two phases. The rate of heat transfer from bubble to bulk liquid is given by:

$$q_{con} = h_{fl} A_i \left(T_{sat} - T_l\right) \tag{18}$$

Where hfi is the interfacial heat transfer coefficient y A_i is the interfacial area per unit of volume. The interfacial condensation rate is given by the following equation:

$$\dot{m}_{con} = \frac{q_{con}}{h_{lv}} \tag{19}$$

The interfacial heat transfer coefficient is calculated by Ranz and Marshall Model [32].

$$h_{fl} = \frac{k_l}{d_b}\left(2 + 0.6\,\mathrm{Re}_b^{1/2}\,\mathrm{Pr}^{1/3}\right) \tag{20}$$

Where the term Re_b is the Reynolds number based on the relative velocity.

Numerical procedure

The previous mathematical model for DSG was solved with the CFD software ANSYS FLUENT v15 [33]. The simulations were carried out in transitory state with time steps between 0.1 and 0.01 s, in a 2D geometry with axial symmetry. The principal boundary conditions are: inlet mass flow, outlet pressure and uniform heat flux on the pipe wall. The values of these conditions were indicated in section 2.1. The thermophysical properties of the liquid phase were estimated as a function of temperature and the properties of the vapor were fixed at the saturation temperature (T_{sat}=530 K). The equations were discretized with a second order upwind scheme and the QUICK scheme was used for volumetric fraction. The solution algorithm (SIMPLEC) was coupled to the volumetric fraction and the convergence was achieved when the residuals of all governing equations were less than 10^{-5}.

Results and Discussion

Mesh independence study

The mesh independence study is presented graphically in Fig. 2, the computational meshes were structured and uniform. Were compared 6 meshes between 10,000 and 37,500 elements, it was concluded that the optimal mesh is that of 20,000 elements, because it has a good concordance with the experimental data, with the lowest computational cost. The selected computational mesh has a minimum orthogonal quality of 1 and its maximum aspect ratio is 5.3.

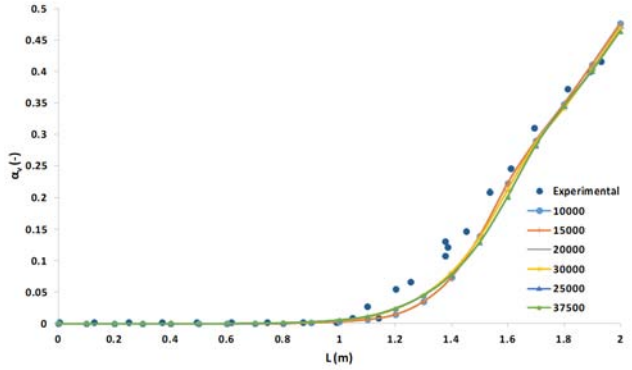

Figure 2. Mesh independence study (profiles of the average αv).

Effect of mass flux

To observe the physical and numerical effects of the mass flux (G), were tested 3 different values: 900, 500 y 200 kg/m^{2}s, named as C1-1 (base), C1-2 and C1-3, respectively.

Case C1-1 (G=900 kg/m^{2}s)

This case reproduces the conditions and experimental data established by Bartolomei and Chanturiya [20] (base case). With this case, were validated the mathematical model and numerical methodology described above. In Figs. 3 and 4, are compared the results of the average volume fraction of the vapor (α_v) and the average temperature of the liquid with the experimental data. The numerical data were obtained by averaging in Y-direction, generating 21 points in X-direction starting from X = 0 m with a separation of 0.1 m.

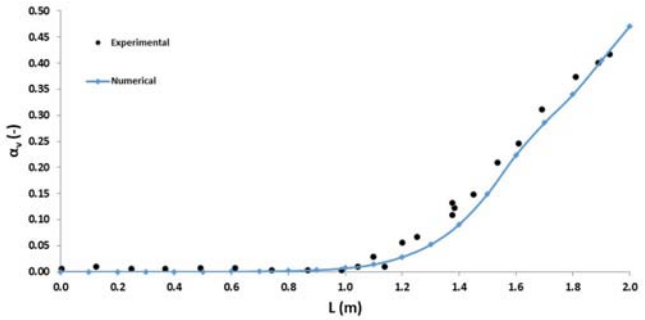

Figure 3. Comparison between the experimental and numerical data for the average αv (-).

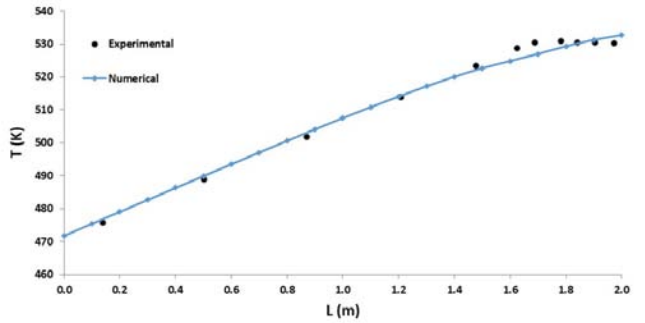

Figure 4. Comparison between the experimental and numerical data for the average temperature of the liquid (K).

Also, it was made a comparison between the experimental and numerical data, for the temperature profile of the liquid located on the axial axis (Fig. 5), the numerical profile reproduces the experimental data, except for the initial part because in the experimental data there are values below the inlet temperature 471.5 K (ΔT_{sub}= 60 K).

From Figs. 3, 4 and 5, it was concluded that the method implemented in this study reproduces satisfactorily the experimental data.

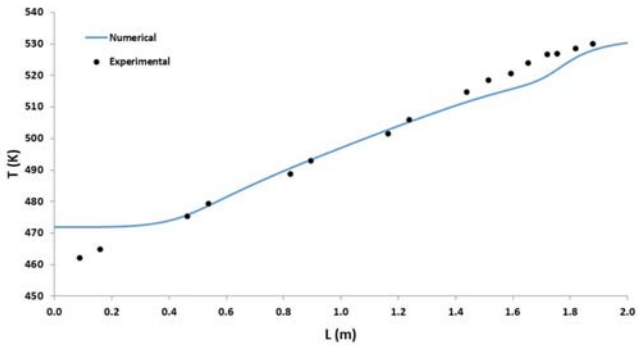

Figure 5. Comparison between the experimental and numerical data for the temperature of the liquid located on the axial axis (R_i= 0 m).

In Fig. 6 are shown the contours of α_v and the contours of the liquid temperature in four sections, where each one shows a quarter of the pipe (0.5 m). The fluid enters the bottom part and transits the sections from left to right (this description is used in all figures of this type). The 4 contours shown in Fig. 6(a) correspond to the αv and it is observed as the fluid changes phase as it passes through of the pipe, the system starts with α_v = 0 and ends with α_v = 0.47. In the first 1.7 m, the fluid presents a bubbly flow topology ($\alpha v \leq 0.3$), in this flow patterns the vapor phase is dispersed in the continuous liquid in the form of bubbles. The Fig. 6(b) shows the contours of the liquid temperature and it is observed how the liquid gains energy as it moves through the pipe. The average outlet temperature of the liquid (T_s) is 532 K, slightly above the T_{sat} because of the T_w.

The characteristics of the contours of Fig. 7 are like those described in Fig. 6, in these contours is shown only the last centimeter of the pipe, with the finality to appreciate more clearly the conditions at the outlet of the fluid. In Fig. 7a it is appreciable that the highest values of the α_v are near the wall, obtaining maximum values of 0.62, and as it approaches the center of the pipe (R_i = 0 m), the values decrease to 0.3. Analyzing these results, it was found that the mass flow of steam and liquid at the outlet was 0.27 and 9.79 kg/min, respectively. The ratio of steam generated mass with respect to the total inlet mass, is defined as steam quality (X_v), which will be equal to 0 in conditions of pure liquid, and equal to 1 in conditions of pure steam, the X_v for this case was 0.027. In Fig. 7b it is observed that the highest temperatures are near the wall with values near to 566 K. As in the contours of αv, the temperatures also tend to decrease as is approach the center of the pipe to a value of 530 K. As can be seen in Fig. 4 at 1.8 m, it was obtained an average temperature of the liquid equal to 530 K, whereas in Fig. 5 can be seen that the liquid has this temperature at 1.97 m.

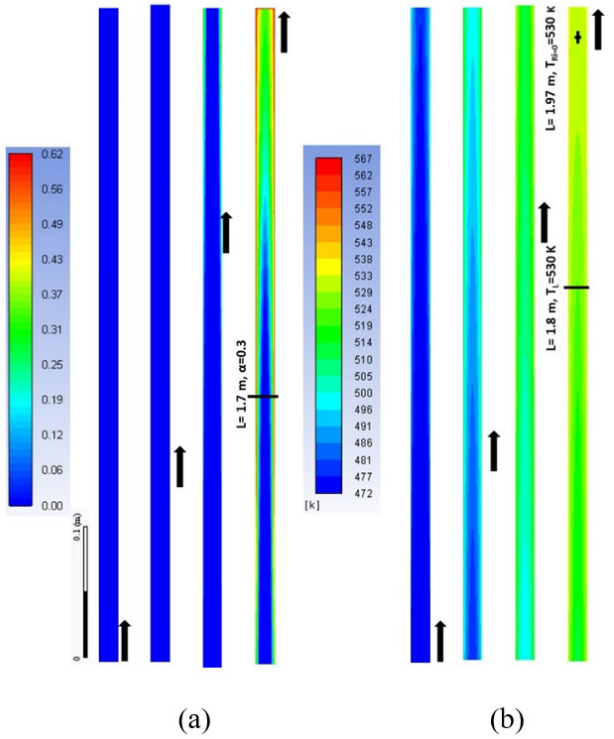

Figure 6. (a) contours of α_v (-) and (b) contours of the liquid temperature (K) for case C1-1.

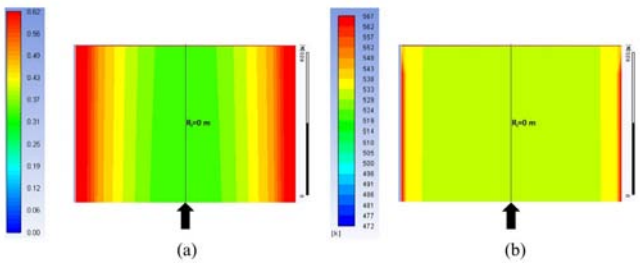

Figure 7. (a) contours of αv (-) and (b) contours of the liquid temperature (K), in the last 0.1 m, case C1-1.

Case C1-2 (G=500 kg/m²s)

In Fig. 8a, are shown the contours of αv, and it is observed that it increases as it moves along the pipe, the αv starts with 0 and ends in 0.83. In the first half of the pipe, it is observed a bubbly flow topology ($\alpha_v \leq 0.3$), from this point the flow topology is churn ($0.3 < \alpha_v < 0.7$). This is distinguished by the chaotic behavior of steam that flows through the liquid which moves principally on the wall of the pipe, this is an intermediate topology between the bubbly and mist flow topology. The mist flow topology ($\alpha_v \geq 0.7$), appears around 1.5 m, it is characterized by the formation of a liquid film adhered to the wall of the pipe and has a continuous steam core, now the liquid phase is dispersed in the continuous vapor in the form of droplets. For this case the X_v was 0.17, and this

value correspond to a mass flow of steam of 0.93 kg/min and 4.66 kg/min for the liquid. In Fig. 9a are shown the contours of αv, again it is appreciated that the highest data are around the wall, with maximum values of 0.88 and tend to 0.7 when approaching the axial zone.

In Fig. 8b are shown the contours of the liquid temperature for this case, and it is observed that the liquid has an average temperature of 530 K from L=1m, from this point the average temperature tends to increase until reaching the 543 K (outlet). In Fig. 9b can be seen that the highest temperatures occur around the wall with values of 732 K, the temperatures also tend to decrease as is approach the center of the pipe to values of 531 K. From graphs 8b and 9b, it can be said that the temperature on the axial axis reaches the T_{sat} around 1.1 m, in this length the temperature of the wall is heated at a rate of 0.12 K/cm, from this point the temperature of the wall begins to increase significantly at the rate of 2.03 K/cm until reaching a temperature of 732 K.

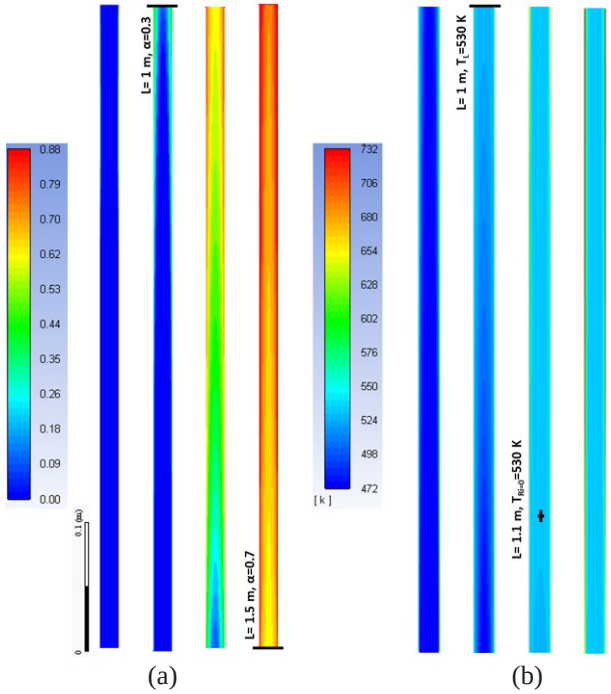

Figure 8. (a) contours of α_v (-) and (b) contours of the liquid temperature (K) for case C1-2.

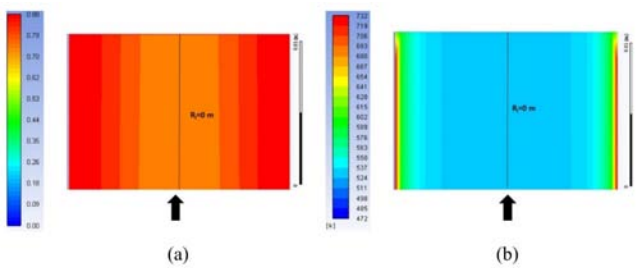

Figure 9. (a) contours of αv (-) and (b) contours of the liquid temperature (K), in the last 0.1 m for case C1-2.

Case C1-3 (G=200 kg/m²s)

In Fig. 10a are shown the contours of αv, its values are between 0 and 0.98. For this case the bubbly flow topology occurs in the first 0.4 m of the pipe ($\alpha_v \leq 0.3$), from this point begins the churn flow, and ends at approximately 0.6 m, after this point the αv is superior to 0.7, therefore, the flow topology is type mist. For this case, the mass flow of steam at the outlet was 1.45 kg/min and 0.79 kg/min for the liquid, whereas the X_v was 0.65. In Fig. 10b is observed a very thin thermal boundary layer adjacent to the wall, whereas the maximum average temperature in the fluid is 570 K, Tw was 2090 K, both at 1.5 m.

In Fig. 11, are shown four temperature contours of one-centimeter height, located in the following positions (a) X=0.5 m, (b) X=1 m, (c) X=1.5 and (d) X=2 m. In Figs. 11a and 11b the liquid temperatures are between 533 and 545 K. In Figs. 11c and 11d the thermal boundary layer adjacent to the wall is more notorious.

Comparison between cases C1-1, C1-2 y C1-3

In Fig. 12, there are 3 representative behaviors of αv profiles. In this work were analyzed different values of G and it was found that the profiles generated with values higher than 900 kg/m²s are like the profile C1-1, It was also observed that profiles generated between 900 and 200 kg/m²s share similarity with the profile C1-2. The profiles generated with values lower than 200 kg/m²s are like the profile C1-3, therefore these 3 cases are representative of the multiple cases that could exist under these conditions, also these profiles provide clear information of the sections where are given the different flow patterns, and it is possible to locate the ONB and NVG points for each case.

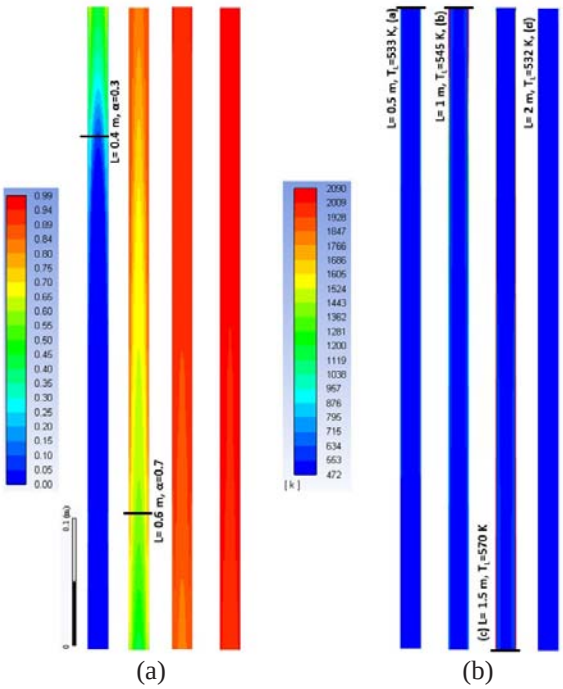

Figure 10. (a) contours of αv (-) and (b) contours of the liquid temperature (K) for case C1-3.

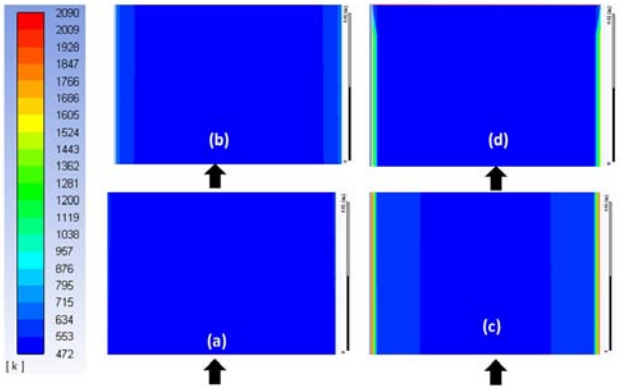

Figure 11. Contours of the liquid temperature (K) for case C1-3. (a) X=0.5 m, (b) X=1 m, (c) X=1.5 m and (d) X=2 m.

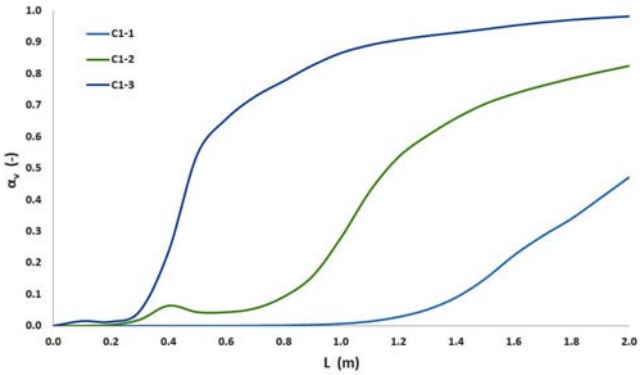

Figure 12. Comparison between average α_v profiles of cases C1-1, C1-2 and C1-3.

The X_v profiles are presented in Fig. 13. As it is appreciable in this figure, the highest values are developed at the end of the pipe in each case. In profile C1-1 the steam generation starts at 0.9 m and ends with X_v of 0.027 (L=2 m). In case C1-2, the profile starts at 0.3 m and ends with X_v of 0.17. In the case C1-3 the steam generation starts at 0.1 m and ends with X_v of 0.65. It is generally appreciated that once steam generation has started, the steam quality increases linearly after a certain length, with respect to the length of the pipe, also that at lower values of G higher values in X_v and that steam generation starts faster. It is important to mention that the highest value in the X_v was 0.65 belonging to a G=200 kg/m^{2}s, since with values lower than this, the simulations present significant errors in the mass balance, principally.

Effect of heat flux (q_w)

The values of q_w are estimated by dividing the energy applied to the fluid through the internal walls of the pipe with respect to the contact area. The following values were applied; 1.14 and 1.71 MW/m^2, named as cases C2-1 and C2-2 respectively.

Case C2-1 (q_w=1.14 MW/m^2)

The contours of αv are shown in Fig. 14a, it is observed the same behavior of the previous cases, starting from 0 and ending with an average α_v of 0.82. The behavior of this case is very similar to the case C1-2, with respect to flow topology, in this case the bubbly flow topology occurs in the first 0.9 m, from this point the churn flow topology predominates until 1.5 m and the mist flow topology is in the last 0.5 m of the pipe. For this case the X_v was 0.15 in the outlet, equivalent to a mass flow of steam of 1.54 kg/min and 8.52 kg/min for the liquid. In Fig. 15a, it is presented the contour of the α_v in the last centimeter of the pipe, and it is seen that in the nucleus the values are 0.71 and near the walls of 0.86 approximately.

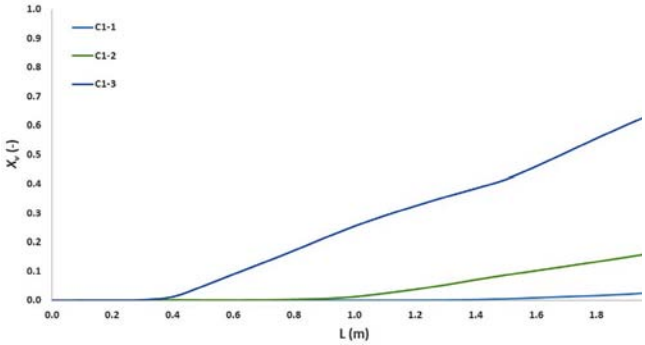

Figure 13. Comparison between X_v profiles (-) of cases C1-1, C1-2 y C1-3.

In Fig. 14b are shown the contours of the liquid temperature for this case. Immediately are shown the average temperatures of the liquid in different points of the pipe, in an L=0.5 m the T_L=505 K, L=1 m the T_L=533 K, L = 1.5m the T_L = 547 K and in the outlet the T_L = 558 K, as it can be seen these temperatures are above the Tsat, this is caused by the elevated temperatures of the pipe wall. In Fig. 15b this is visualized more clearly, this is the contour of the liquid temperatures in the last centimeter of the pipe, and can observe that the highest temperatures occur near the wall, with maximum values of 909 K and the minors in the center of the pipe, with values of 531 K.

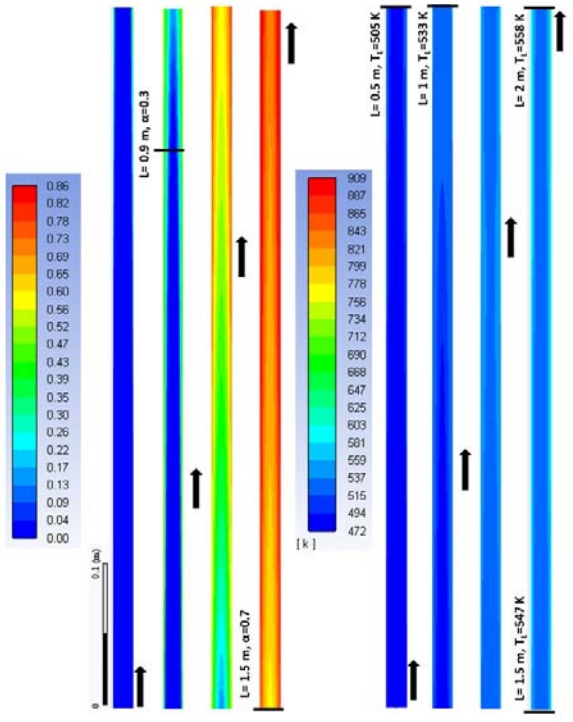

Figure 14. (a) Contours of α_v (-) and (b) contours of the liquid temperature (K) for case C2-1.

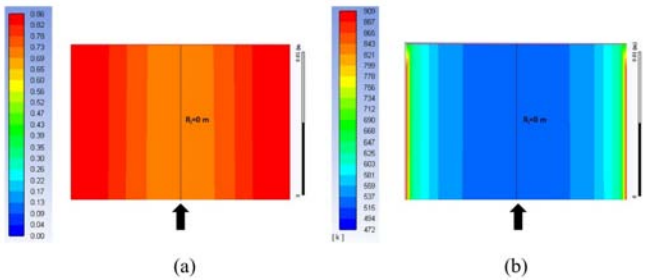

Figure 15. (a) Contours of αv (-) and (b) contours of the liquid temperature (K), in the last 0.1 m for case C2-1.

Case C2-2 (qw = 1.71MW/m²)

In Fig. 16a are shown the contours of the α_v of this case, the αv starts with a value of 0 and ends with 0.91. The bubbly flow topology ends at 0.6 m approximately and from this point to 1.2 m the flow topology is churn, and the rest of the pipe is mist. For this case, the mass flow of steam at the outlet was 2.77 kg/min and 7.28 kg/min for the liquid, with an X_v of 0.28. In Fig. 16b are shown the contours of the liquid temperature for this case and there aren't significant changes in the contours shown, this is because the predominant temperature in the liquid is lower than the maximum temperature reported in the wall. In Fig. 17d, it is observed a very thin layer near the wall with temperatures between 1250 K and 2230 K approximately.

In Fig. 17 are shown 4 contours of one centimeter in length, located in the following positions (a) X=0.5 m, (b) X=1 m, (c) X=1.5 m and (d) X=2 m. From point (a) to point (b) the average temperatures of the liquid are between 518 and 553 K, and the T_w of 607 to 730 K, respectively, now at point (c) the T_L is 570 K, with a Tw of 1250 K and finally at point (d) the T_L was 567 K, with a T_w around 2000K.

Comparison between Cases: C1-1, C2-1 and C2-2

Next, it is made a comparison between 3 profiles of the α_v (Fig. 18). The vapor generation for *C1-1* starts in X=0.9 m ending with α_v=0.47. The Case C2-1 starts with steam generation at approximately 0.1 m and ends with an α_v of 0.82 and finally the case C2-2 initiates steam generation between 0 and 0.1 m and ends with α_v of 0.9. Therefore, it is appreciated that by increasing qw, steam generation also increases and starts faster. A comparison was made between the 3 profiles of the X_v (Fig. 19). It is observed the same behavior described in Fig. 18, X_v evaluated at 2 m for C1-1, C2-1 and C2-2 were 0.027, 0.15 and 0.28, respectively. The heat flux of case C2-2 (1.71 MW/m²) was considered as the maximum limit q_w for this parametric study, that is, higher values generate errors in mass balances and divergence states.

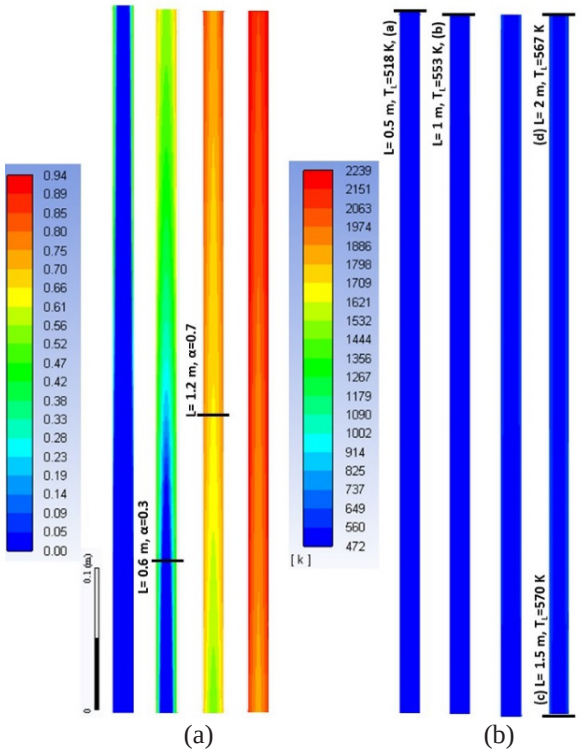

Figure 16. (a) Contours of α_v (-) and (b) contours of the liquid temperature (K) for case C2-2.

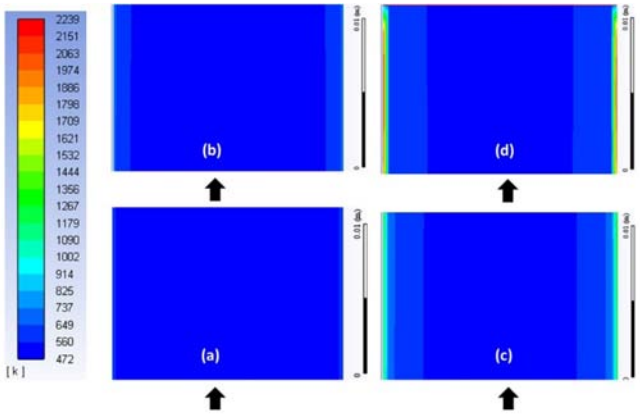

Figure 17. Contours of the liquid temperature (K). (a) X=0.5 m, (b) X=1 m, (c) X=1.5 m, (d) X=2 m for case C2-2.

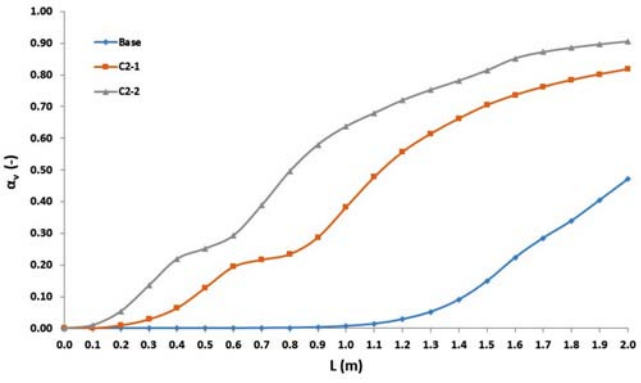

Figure 18. Comparison between αv profiles (-) of C1-1, C2-1 and C2-2.

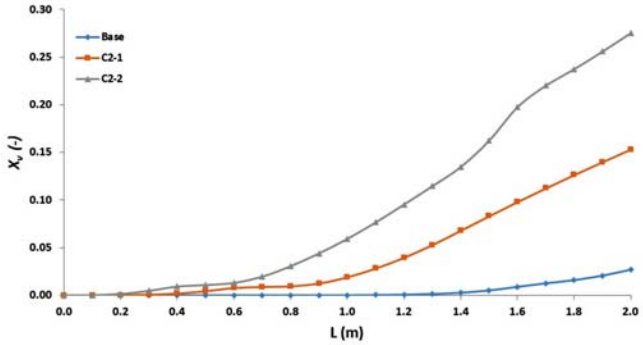

Figure 19. Comparison between Xv profiles (-), cases base, C2-1 and C2-2.

Effect of tube length (L)

This section consists to observe the effect of the heat transfer area incrementing the tube length (L). Three lengths were analyzed: 4, 8 and 14 m (Cases C3-1, C3-2 and C3-3 respectively).

Case C3-1 (L=4 m)

To better appreciate the contours of αv and the contours of the liquid temperature, the length of the pipe was divided into 8 sections of 0.5 m, the fluid inlet is on the lower left side and the outlet on the upper right side.

In Fig. 20 the contours of the αv of this case are shown, starting at 0 (inlet) and ending with an average value of 0.881 (outlet), it is observed the same behavior of the previous cases. In this case the bubbly flow topology ($\alpha_v \leq 0.3$), occurs in the first 1.7 m, from this point the churn flow topology ($0.3 < \alpha_v < 0.7$), predominates until 2.6 m and the mist flow topology ($\alpha_v \geq 0.7$), is in the last 1.4 m of the pipe. For this case, the mass flow of steam at the outlet was 2.14 kg/min and 7.92 kg/min for the liquid, with an X_v of 0.21.

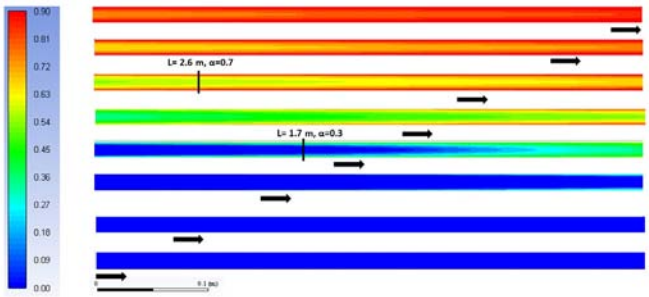

Figure 20. Contours of αv (-) for case C3-1.

The liquid temperature contours for this case are shown in Fig. 21, like the previous cases, the zones with the highest temperatures are near the walls, and those of lower temperature are around R_i = 0 m, it was obtained a T_s of 543 K and its value in R_i = 0 m was T_{sat}.

In Fig. 22, can be seen that the generation of steam begins significantly and under a constant slope (red line) around 1.97 m (gray line), values of X_v were taken from 3 m and these data were adjusted to a straight-line model. The slope of this equation is 0.0934 and its ordinate in the origin is -1607, the r^2 is 0.9999. These values guarantee that steam generation is constant from this point. Another contribution of this equation is that it allows us to predict the length where the mass of the liquid is completely exhausted, it was found that at L = 12.43 m the X_v = 1, this result will be validated later with the case C3-3.

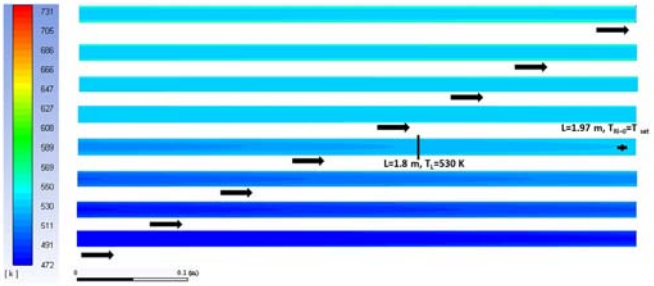

Figure 21. Contours of the liquid temperature (K) for case C3-1.

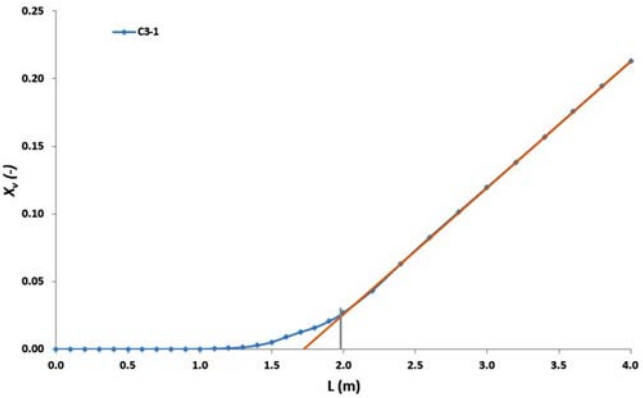

Figure 22. Profile of Xv (-) for case C3-1.

Case C3-2 (L=8 m)

In Fig. 23 the contours of the αv of this case are shown (from L = 4 to L = 8 m, because the first 4 m were described in case C3-1), starting with 0.881 (final condition of case C3-1) and ending with an average value of 0.975, the flow topology that dominates this section is of type mist ($\alpha_v \geq 0.7$). The mass flow of steam at the outlet was 5.78 kg/min and 4.28 kg/min for the liquid, with an X_v of 0.57.

Figure 23. Contours of αv (-), case C3-2.

The liquid temperature contours for this case are shown in Figs. 24 and 25, The inlet temperature of the liquid was 543 K and the it was reached the T_{sat} in the 6.6 m and from this point the liquid temperature remained constant until the end of this section.

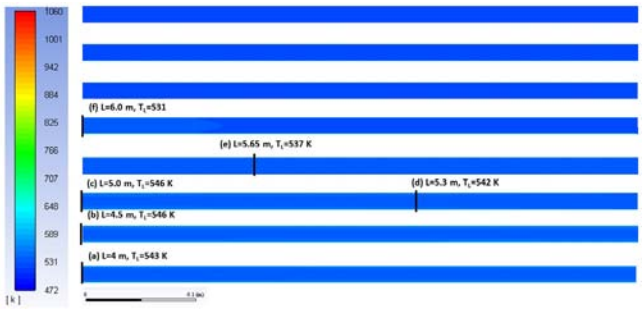

Figure 24. Contours of the liquid temperature (K), case C3-2.

In Fig. 26, are shown 6 contours of 1 cm taken at different points. The contour (a) in X=4 m, (b) X=4.5 m, (c) X=5 m, (d) X=5.3 m, (e) X=5.65 m y (f) in X=6 m. In each of these points the central contour is the T_{sat} of the system. From point (a) to point (c) the temperature of the wall increases from 734 to 900 K. Between point (c) and (d) the opposite occurs, this contour increases to the point (e), coming to cover most of the pipe, except for small areas near the walls. On the other hand, it is seen that the temperature of the wall continues to increase until reaching its maximum value (1060 K) located at point (e), from this point the temperature in the wall decreases, at point (f) the temperature on the wall is 1041 K.

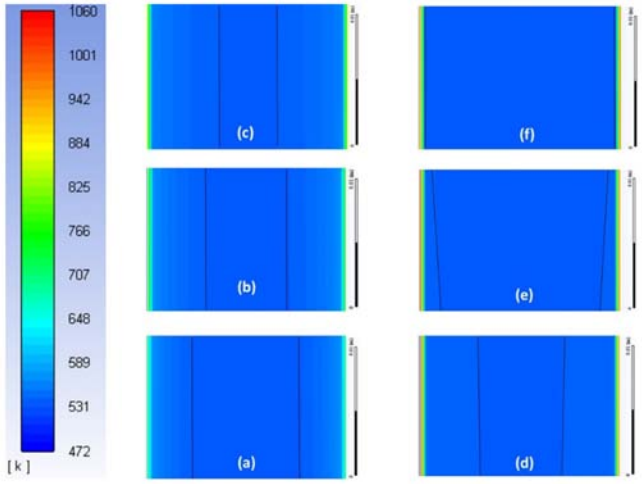

Figure 25 Contours of the liquid temperature (K), (a) X=4 m, (b) X=4.5 m, (c) X=5 m, (d) X=5.3 m, (e) X=5.65 m and (f) X=6 m, case C3-2.

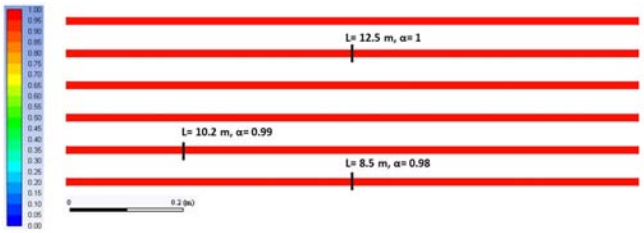

Figure 26 Contours of α_v (-) for case C3-3.

Case C3-3 (L=14 m)

This case is a continuation of case C3-2, the contours are presented from L = 8 m to L = 14 m. The length corresponding to this case was divided into 6 sections of 1 m. As can be seen in Fig. 26 the contours do not show a significant change in the color scale, because the αv is very similar in the last 6 m of pipe, this case starts with αv of 0.975 (final condition of case C3-2), at 8.5 m the α_v is 0.98, at 10.2 m the α_v is 0.99 and from the 12.5 m the αv is 1, approximately in this region it is reached the X_v of 1from this point the flow is single phase steam, the mass flow of steam at the outlet is 10.01 kg/min, and is equivalent to the inlet mass flux of 900 kg/m²s.

Comparison between cases: C1-1, C3-1, C3-2 and C3-3

Next, there will be a general analysis of the behavior of the phase change phenomenon that occurred in these 4 cases. As previously described, case C3-1 corresponds to an L = 4 m, of which the first 2 m correspond to the base case (C1-1), To perform a detailed analysis, it has been separated into two sections, the first corresponding to case C1-1 and the second to the results of case C3-1.

In Fig. 27 it is presented a temperature profile from L = 0 m to L = 14 m, in this profile appears the wall temperature (red line), the liquid temperature in Ri = 0 m, the average liquid temperature (gray line and blue line respectively), the steam temperature in Ri = 0 m, the temperature average steam (yellow line and orange line respectively), the vertical black lines separate the aforementioned cases, the vertical green and blue lines indicate important changes in the behavior of the profiles. The Fig. 28 presents the profiles of α_v for different cases with L=14 m. To explain the behavior predicted by the mathematical model, the Fig. 29 shows the graphical representation of equation (16), as a function of α_v. On the other hand, the profile of X_v for the tube a length of 14 m (separated by cases) is presented in Fig. 30.

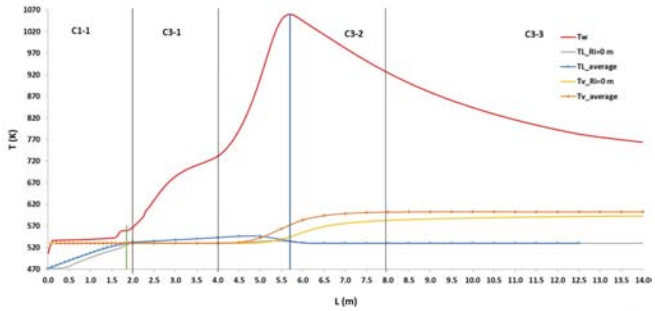

Figure 27. Comparison between temperature profiles for liquid, vapor and wall temperatures (K) for different cases (C1-1, C3-1, C3-2 and C3-3).

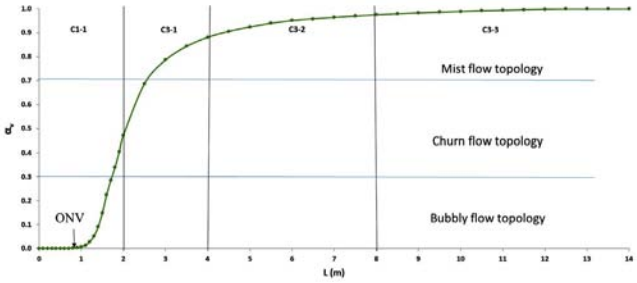

Figure 28. Profile of α_v (-) for different Cases (C1-1, C3-1, C3-2 and C3-3).

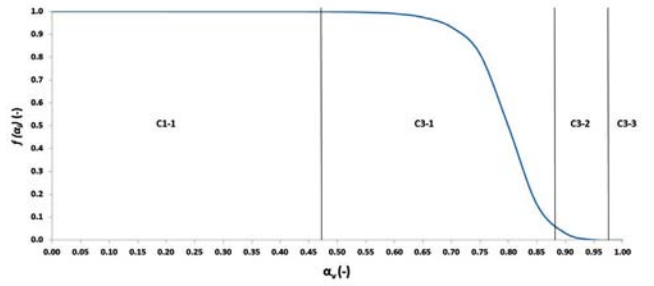

Figure 29. Behavior of f(α_v) for different cases.

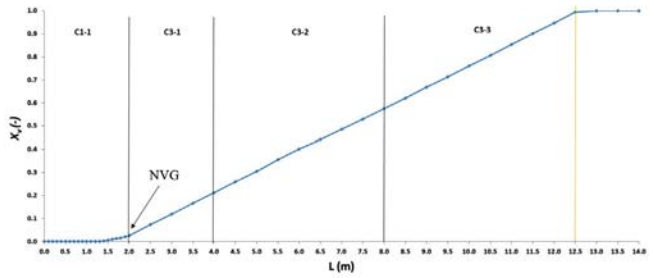

Figure 30. Profile of Xv (-) for different Cases (C1-1, C3-1, C3-2 and C3-3).

Continuing with Fig. 27, the first case to describe is C1-1 or base case, this case develops in the first 2 m of the pipe, the flow topology that predominates in this section is the bubbly type (Fig. 28). In this region the T_w increases slightly, at a rate of 0.3 K/cm, starting from 506 K and ending at 567 K. The behavior of the steam temperature for both profiles (yellow and orange), remain constant along this length at a temperature of 530 K (T_{sat} of the system), it is to be expected that the mass of steam in these conditions does not gain energy, because the function $f(\alpha_l)$ (characteristics of the modified RPI model), is equal to 1 evaluated in α_v of 0.47 (Fig.29), this means that the qw is given to the liquid phase, through the 3 mechanisms described by Eq. 15. With the help of Fig. 30 we can see that the X_v starts to increase from a L = 1.2 m, obtaining 0.027 at 2 m, this indicates that there is a minuscule amount of steam in this first section. The temperature profiles of the liquid show differences, the blue line is above the temperature evaluated in R_i = 0 m, because the fluid near the wall is at higher temperatures and this causes its average value to increase, both profiles experience an increase in temperature, both start at 471.5 K and end at T_{sat} approximately, this region can be classified as the sensible heat stage with subcooled boiling.

In case C3-1 the first thing that is observed is the rapid increase of T_w (Fig. 27), for this section the T_w reaches 731 K and is heated to a ratio of 0.82 K/cm, 2.7 times faster than the previous section. This is because in this region the fluid is at T_{sat}, therefore the energy supplied to it is used to promote the phase change. In this section there are two flow topologies, the first is the churn topology and it ends at 2.6 m, from this point the mist type appears, the αv at the end of this section was 0.88 (Fig. 29), the X_v to 4 m was 0.21 (Fig. 30). We can see that the profiles of the steam temperatures are still maintained at the Tsat, as well as the liquid profile at R_i = 0 m, the average temperature of the liquid tends to increase from 533 to 543 K, effect of the Tw.

The next case is C3-2, in this case several interesting phenomena appear, In Fig. 27 it can be seen that the T_w profile increases as the fluid advances, reaching a maximum value of 1060 K at an L of 5.7 m, in this section the T_w was increased to a ratio of 1.94 K/cm, 2.36 times faster than the C3-1 case, after this point it is observed that the profile decreases almost linearly reaching a temperature of 926 K at L = 8 m, the cooling of the wall is given at a ratio of 0.58 K/cm. Another important behavior is the increase in steam temperature which starts around 4.5 m, with αv of 0.9, where its corresponding value in (1-$f(\alpha_l)$)= 0.963 (Fig. 29), this means that q_w is mostly destined to the vapor phase in the form of convective heat, caused that the liquid does not gain energy through q_w, caused that the average temperature of the liquid decreases. The X_v evaluated in 4.5 m is 0.26 (Fig. 30), this means that at this point the system has 74% of the mass in the liquid phase to the T_{sat}, with a mist flow topology (Fig. 28), from this point this liquid mass in the form of drops will change its mechanism of energy exchange, now the surrounding vapor by means of convection will end with the phase change, caused the cooling in the wall. The average temperature and in R_i = 0 m of the steam increase from 530 K to 602 K and 583 K respectively.

The behavior of case C3-3 is like the second part of case C3-2, a cooling situation. The T_w decreases to 765 K at a rate of 0.27 K/cm, the steam temperature at L = 14 m is around 600 K. The α_v and the X_v are equal to 1 and are obtained around 14.5 m, in case C3-1 it was predicted that at an L = 12.43 could occur the total phase change, the error was 0.56%.

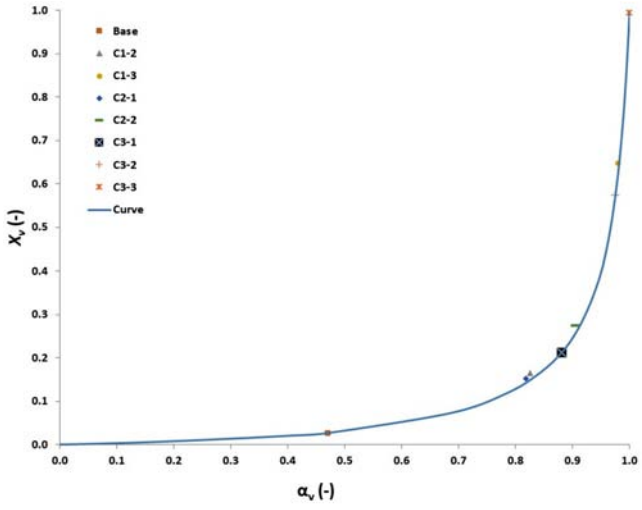

Figure 31. Relationship between αv and Xv for each case.

Relationship between αv and X_v for each case.

In Fig. 31, the maximum values α_v for each case are related to their corresponding value of X_v. The adjustment line of Fig. 32 was extracted from the data obtained in case C3-3, it shows an exponential behavior when αv approaches to 1

(this behavior is due to the difference in densities between the phases). It is important to mention that the pairs of α_v and X_v, for each case adapt well to the curve, which means that for each value of αv there will be a single value of Xv, independently of which parameter is modified, except for the system pressure.

Conclusions

The numerical strategy implemented in this work, reproduced satisfactorily the experimental data reported in literature. From the results we obtain the following conclusions:

1. The numerical methodology was able to determine what conditions can produce steam qualities of 100%.
2. Decrease the mass flux (G) and increase the heat flux in the wall (q_w) causes the system to increase the X_v and that ONV and NVG points start at a shorter length, causing the maximum X_v for these cases to be 0.65 and 0.28 respectively.
3. Once the NVG point has been reached, the steam generation is constant (linear), under this characteristic it is possible to predict at what length will be pure steam (X_v = 1).
4. Increasing the length of the pipe (L) generated the best numerical stability to obtain an X_v of 1.

Acknowledgment

The authors are grateful to the National Council of science and technology (CONACyT) and to the University of Sonora (UNISON) for the support provided for the realization of this work.

Nomenclature

R_i	Internal pipe radius, m
L	Pipe length, m
G	Mass flux, kg m^{-2} s^{-1}
P	Pressure, N m^{-2}
T_e	Inlet temperature of the liquid, K
T_s	Outlet average temperature of the liquid, K
$\vec{u}$	Velocity, m s^{-1}
H	Specific enthalpy, J kg^{-1}
ṁ	Mass flow rate, kg s^{-1}
$\vec{g}$	Acceleration due to gravity, m s^{-2}
t	Time, s
$\overrightarrow{F_D}$	Drag force, N
$\overrightarrow{F_L}$	Lift force, N
$\overrightarrow{F_W}$	Wall lubrication force, N
$\overrightarrow{F_{TD}}$	Turbulent dispersion force, N
q	Heat flux, W m^{-2}
A	Area, m^2
A_b	Area of influence, m^{-2}
1- A_b	Area covered with fluid, m^{-2}
h	Heat transfer coefficient, W m^{-2} s^{-1}
T_w	Wall temperature, K
T_l	Liquid temperature, K
T_v	Vapor temperature, K
d_{bw}	Bubble departure diameter, m
d_b	Bubble diameter, m
N_a	Nucleation site density, No. of sites m-2
f	Bubble departure frequency, s-1
Ja	Jacob Number, -
T_{sat}	Saturation temperature, K
h_{lv}	Latent heat of vaporization, J kg^{-1}
Cp	Specific heat, J kg^{-1} K^{-1}
k	Thermal conductivity, W m^{-1} K^{-1}
t_w	Waiting period, s
V	Volumetric flow, m^3 s^{-1}
R_c	Critical cavity size base on wall superheat, m
d_{bo}	Bubble boiling diameter, m
$\lvert\overline{u_v} - \overline{u_l}\rvert$	Relative velocity between phases (vapor and liquid), m s^{-1}
A_i	Interfacial area per unit of volume, m^2 m^{-3}
Re_b	Reynolds Number based on relative velocity, -
Pr	Prandtl Number, -
Re	Reynolds Number, -
X_v	Ratio of the generated mass of steam with respect to the total mass, -
r^2	Correlation coefficient, -

Subscripts

k	Phase k
i	Phase i
W	Wall
c	Convective
q	quenching
e	Evaporative
Sub	Subcooling
l	Liquid
v	Vapor
fi	Interfacial

Greek letters

α	Volume fraction, -
ρ	Density, kg m^{-3}
μ	Viscosity, kg s^{-1} m^{-1}
ΔT_{sub}	Subcooled temperatura (T_w-T_{sat}), K
λ	Thermal diffusivity, m^2 s^{-1}
φ	Contact angle, deg. / °
σ	Surface tension, N m^{-1}
μ^{bt}	Viscosity due to bubble induced turbulence, kg s^{-1} m^{-1}
k	Turbulent kinetic energy,
ε	Rate of dissipation,

Abbreviations

CST	Concentrating Solar Thermal Systems
CST	Central Solar Tower
DSG	Direct Steam Generation
CFD	Computational Fluid Dynamics
VOF	Volume of Fluid
RPI	Rensselaer Polytechnic Institute
ONV	Onset of Nucleate Boiling
NVG	Net Vapor Generation

References

[1] *Renewable Energy Technologies: Cost Analysis Series*, Volume 1: Power Sector Issue 2/5, Concentrating Solar Power. IRENA, June (2012).

[2] Hirsch, T., Feldhoff, J.F., Hennecke, K., Pitz-Paal, R., 2014. *Advancements in the field of direct steam generation in linear solar concentrators - a review*. Heat Transfer Eng. 35, 258–271.

[3] Gonzalez-Roubaud, E., Pérez-Osorio, D., Prieto, C., 2017. *Review of commercial thermal energy storage in concentrated solar power plants: steam vs. molten salts*. Renew. Sustain. Energy Rev. 80, 133–148.

[4] Prieto Cristina, Rodríguez Alfonso, Patiño David, Cabeza Luisa F., 2018, *Thermal energy storage evaluation in direct steam generation solar plants*, Solar Energy. 159, 501–509.

[5] Aguilar-Gastelum F., Moya S. L., Cazarez-Candiaa O., Valenzuela L., 2014. *Theoretical study of direct steam generation in two parallel pipes*. Energy Procedia, 2265– 2274.

[6] Xu Rong, Wiesner Theodore F., 2015. *Closed-form modeling of direct steam generation in a parabolic trough solar receiver*. Energy, 163–176.

[7] Ravelli S., Franchini G., Perdichizzi A., Rinaldi S., Valcarenghi V.E., 2016. *Modeling of Direct Steam Generation in Concentrating Solar Power Plants*. Energy Procedia, 464–471.

[8] Cundapí Roger, Moya Sara L., Valenzuela Loreto, 2017. *Approaches to modelling a solar field for direct generation of industrial steam*. Renewable Energy. 666–681.

[9] Lobon, D.H., Baglietto, E., Valenzuela, L., Zarza, E., 2014. *Modeling direct steam generation in solar collectors with multiphase CFD*. Appl. Energy 113, 1338–1348.

[10] Lobon, D.H., Valenzuela, L., Baglietto, E., 2014. *Modeling the dynamics of the multi- phase fluid in the parabolic-trough solar steam generating systems*. Energy Convers. Manage. 78, 393–404.

[11] Dinsenmeyer R., Fourmigué, J.F. Caney N., Marty P., 2017. *Volume of fluid approach of boiling flows in concentrated solar plants*. International Journal of Heat and Fluid Flow, 177–191.

[12] Yang, Z., Peng, X.F., Ye, P., 2008. *Numerical and experimental investigation of two phase flow during boiling in a coiled tube*. Int. J. Heat Mass Transf. 51, 1003–1016.

[13] Krepper, E., Končar, B., Egorov, Y., 2007. *CFD modelling of subcooled boiling-Concept, validation and application to fuel assembly design*. Nucl. Eng. Des. 237, 716–731.

[14] Li, H., Vasquez, S.A., Punekar, H., Muralikrishnan, R., 2011. *Prediction of boiling and critical heat flux using an eulerian multiphase boiling model*. In: ASME 2011 International Mechanical Engineering Congress and Exposition. pp. 463–476.

[15] Cheung S.C.P., Vahaji S., Yeoh G.H., Tu J.Y., 2014. *Modeling subcooled flow boiling in vertical channels at low pressures – Part 1: Assessment of empirical correlations*. International Journal of Heat and Mass Transfer, 736–753.

[16] Zhang, R., Cong, T., Tian, W., Qiu, S., Su, G., 2015. *Effects of turbulence models on force convection subcooled boiling in vertical pipe*. Ann. Nucl. Energy 80, 293–302.

[17] Braz Filho, F.A., Ribeiro, G.B., Caldeira, A.D., 2016. *Prediction of subcooled flow boiling characteristics using two-fluid Eulerian CFD model*. Nucl. Eng. Des. 308, 30–37.

[18] Chaitanya R. Mali, V. Vinod, Ashwin W. Patwardhan., 2017. *Comparison of phase interaction models for high pressure subcooled boiling flow in long vertical tubes*. Nuclear Engineering and Design. 337–359.

[19] Kurul, N., Podowski, M.Z. 1991. *On the modeling of multidimensional effects in boiling channels*. Proceedings of the 27th National Heat Transfer Conference. pp. 301–314.

[20] Bartolomei, G.G., Chanturiya, V.M., 1967. *Experimental study of true void fraction when boiling subcooled water in vertical tubes*. Therm. Eng. 14, 123–128.

[21] Ishii, M., Zuber, N., 1979. *Drag coefficient and relative velocity in bubbly, droplet or particulate flows*. AIChE J. 25, 843–855.

[22] Moraga, F.J., Bonetto, F.J., Lahey, R.T., 1999. *Lateral forces on spheres in turbulent uniform shear flow*. Int. J. Multiph. Flow 25, 1321–1372.

[23] Antal, S.P., Lahey, R.T., Flaherty, J.E., 1991. *Analysis of phase distribution in fully developed laminar bubbly two-phase flow*. Int. J. Multiph. Flow 17, 635–652.

[24] Lopez de Bertodano M., 1991. "*Turbulent Bubbly Flow in a Triangular Duct*". Ph.D. Thesis. Rensselaer Polytechnic Institute, Troy, New York.

[25] Del Valle, V.H., Kenning, D.B.R., 1985. *Subcooled flow boiling at high heat flux*. Int. J. Heat Mass Transf. 28, 1907–1920.

[26] Mikic, B.B., Rohsenow, W.M., 1969. *A new correlation of pool-boiling data including the effect of heating surface characteristics*. J. Heat Transfer 91, 245–250.

[27] Cole, R., 1967. *Bubble frequencies and departure volumes at subatmospheric pressures*. AIChE J. 13, 779–783.

[28] Kocamustafaogullari, G. and Ishii, M., 1983. "*Interfacial area and nucleation site density in boiling systems*", Int. J. Heat Mass Transfer, 26, 1377-1387.

[29] Lavieville J., Quemerais E., Mimouni S., Boucker M. and Mechitoua N., 2005. "*NEPTUNE CFD V1.0 Theory Manual*". EDF.

[30] Launder B. E. and Spalding D. B., 1972. *Lectures in Mathematical Models of Turbulence*. Academic Press, London, England.

[31] Sato, Y., Sadatomi, M., Sekoguchi, K., 1981. *Momentum and heat transfer in two-phase bubble flow-I. Theory*. Int. J. Multiph. Flow 7, 167–177.

[32] Ranz, W.E., Marshall, W.R., 1952. *Evaporation from drops*. Chem. Eng. Prog. 48, 141446.

[33] ANSYS Inc. (US), 2013. ANSYS Fluent Theory Guide 15317, 565–572.